Dual-energy multidetector-row computed tomography of the hepatic arterial system: optimization of energy and material-specific reconstruction techniques

Marin, Daniele ; Caywood, Devin T ; Mileto, Achille ; Reiner, Caecilia S ; Seaman, Danielle M ; Patel, Bhavik N ; Boll, Daniel T ; Nelson, Rendon C

Abstract: PURPOSE To investigate the optimal dual-energy reconstruction technique for the visualization of the hepatic arterial system during dual-energy multidetector computed tomographic (MDCT) angiography of the liver. MATERIALS AND METHODS Twenty-nine nonconsecutive patients underwent dual-energy MDCT angiography of the liver. Synthesized monochromatic (40, 50, 60, and 80 keV) and iodine density data sets were reconstructed. Aortic attenuation, noise, and contrast-to-noise ratio (CNR) were measured. In addition, volume-rendered images were generated and qualitatively assessed by 2 independent readers, blinded to technique. The impact of body size on the readers' scores was also assessed. RESULTS Aortic attenuation, noise, and CNR increased progressively with decreasing keV and were significantly higher between 40 and 60 keV ($P < 0.001$). There was a significant improvement of readers' visualization of arterial anatomy at lower monochromatic energies ($P < 0.001$). Iodine density images yielded significantly higher CNR compared with all monochromatic data sets ($P < 0.001$). However, iodine density images were scored nondiagnostic by the 2 readers. CONCLUSIONS Synthesized monochromatic images between 40 and 60 keV maximize the magnitude of arterial enhancement and improve visualization of hepatic arterial anatomy at dual-energy MDCT angiography of the liver. Larger body sizes may counteract the benefits of using lower monochromatic energies.

DOI: https://doi.org/10.1097/RCT.0000000000000259

Originally published at:
Marin, Daniele; Caywood, Devin T; Mileto, Achille; Reiner, Caecilia S; Seaman, Danielle M; Patel, Bhavik N; Boll, Daniel T; Nelson, Rendon C (2015). Dual-energy multidetector-row computed tomography of the hepatic arterial system: optimization of energy and material-specific reconstruction techniques. Journal of Computer Assisted Tomography, 39(5):721-729.
DOI: https://doi.org/10.1097/RCT.0000000000000259

Dual-Energy Multidetector-Row Computed Tomography of the Hepatic Arterial System: Optimization of Energy and Material-Specific Reconstruction Techniques

Daniele Marin, MD, Devin T. Caywood, MD, Achille Mileto, MD, Caecilia S. Reiner, MD, Danielle M. Seaman, MD, Bhavik N. Patel, MD, Daniel T. Boll, MD, and Rendon C. Nelson, MD

Purpose: To investigate the optimal dual-energy reconstruction technique for the visualization of the hepatic arterial system during dual-energy multidetector computed tomographic (MDCT) angiography of the liver.

Materials and Methods: Twenty-nine nonconsecutive patients underwent dual-energy MDCT angiography of the liver. Synthesized monochromatic (40, 50, 60, and 80 keV) and iodine density data sets were reconstructed. Aortic attenuation, noise, and contrast-to-noise ratio (CNR) were measured. In addition, volume-rendered images were generated and qualitatively assessed by 2 independent readers, blinded to technique. The impact of body size on the readers' scores was also assessed.

Results: Aortic attenuation, noise, and CNR increased progressively with decreasing keV and were significantly higher between 40 and 60 keV ($P < 0.001$). There was a significant improvement of readers' visualization of arterial anatomy at lower monochromatic energies ($P < 0.001$). Iodine density images yielded significantly higher CNR compared with all monochromatic data sets ($P < 0.001$). However, iodine density images were scored nondiagnostic by the 2 readers.

Conclusions: Synthesized monochromatic images between 40 and 60 keV maximize the magnitude of arterial enhancement and improve visualization of hepatic arterial anatomy at dual-energy MDCT angiography of the liver. Larger body sizes may counteract the benefits of using lower monochromatic energies.

Key Words: dual-energy multidetector CT (MDCT), hepatic arterial system, volume-rendering technique, synthesized monochromatic images, contrast-to-noise ratio (CNR)

(*J Comput Assist Tomogr* 2015;00: 00–00)

Recent technologic advances in dual-energy multidetector-row computed tomography (MDCT) allow near-simultaneous acquisition of high- and low-energy data sets (80 and 140 kVp), which can be used for the reconstruction of material density and synthesized monochromatic images in the projection domain.[1,2] By interrogating the changes in attenuation over a discrete range of energies (from 40 to 140 keV), synthesized monochromatic images have the potential to optimize image contrast based on individual patient's body habitus or the specific clinical question, while simultaneously mitigating the detrimental effects of noise and beam hardening.[1–3]

From the Department of Radiology, Duke University Medical Center, Durham, NC.

Received for publication January 20, 2015; accepted March 12, 2015.

Reprints: Daniele Marin, MD, Department of Radiology, Duke University Medical Center, Durham, Box 3808 Erwin Rd, NC 27710 (e-mail: danielemarin2@gmail.com).

One author of the study (R.C.N.) is a medical consultant to GE Healthcare. All other authors declare no conflict of interest.

Recent evidence has suggested that, for most abdominal and vascular imaging applications, monochromatic images between 60 and 70 keV may provide an optimal trade-off between enhanced iodine contrast and acceptable noise.[1–4] However, there is still a relative paucity of data regarding the ideal monochromatic energy level for volume rendering postprocessing techniques of MDCT angiography examinations. This gap in knowledge has significant clinical implications as volume-rendered images have become a key component of routine MDCT angiography examinations, to the point where review of the transverse reconstructions may be regarded as an important adjunctive tool in the overall study interpretation.

The purpose of this study was to investigate the optimal dual-energy reconstruction technique for the visualization of the hepatic arterial system during MDCT angiography of the liver.

MATERIALS AND METHODS

This retrospective, single-center, Health Insurance Portability and Accountability Act–compliant study was approved by the institutional review board of Duke University, and a waiver of informed consent was obtained.

The authors had full control of the data and the information submitted for publication. One author of the study (blinded to the review process) is a medical consultant to GE Healthcare. The lead author (blinded to the review process), who is not an employee of or a consultant for GE Healthcare, had control of inclusion of any data and information that might present a conflict of interest.

Study Population

A dual-energy MDCT Web-based thin client database (Advantage Windows, AW Server 2, release 5.5; GE Healthcare, Inc, Waukesha, WI) was retrospectively searched for all consecutive patients who underwent arterial phase MDCT of the liver between March 1, 2011, and July 18, 2011. The exclusion criteria included any unexpected deviations from the MDCT protocol or contrast-medium injection technique, equipment malfunction, or unexpectedly low arterial contrast (<150 Hounsfield units [HU]). No patients recruited were ultimately excluded for any of these reasons.

The study population consisted of 29 patients (mean age, 57; age range, 32–68 years), including 18 men and 11 women. The mean patient body weight and body mass index (defined as the weight in kilograms divided by height in meters squared) were 84 ± 15 kg (range, 45-150 kg) and 28 ± 6 kg/m^2 (range, 18–51 kg/m^2), respectively.

MDCT Technique

All MDCT examinations were performed using a single-source dual-energy 64-section MDCT scanner with fast kilovolt-peak switching technology (Discovery CT750 HD; GE Healthcare,

TABLE 1. MDCT Acquisition and Reconstruction Parameters

MDCT Parameters	Dual-Energy Scan
Detector configuration, mm	64 × 0.625
Tube voltage, kV	80/140
Tube current, mA	640
Gantry revolution time, sec	0.6
Acquisition mode	Helical
Helical Pitch	1.375
$CTDI_{vol}$, mGy	15.6
Reconstructed section thickness, mm	1.00
Reconstructed section increment, mm	1.00
Reconstruction algorithm	Projection-based material decomposition
Reconstruction kernel	Soft tissue

$CTDI_{vol}$ indicates volume CT dose index.

Inc). Each patient was scanned in the following intravenous contrast-medium administration during the arterial and hepatic venous phases. To determine the optimal scanning delay for the arterial phase, an automatic bolus-tracking technique (SmartPrep; GE Healthcare, Inc) was used to assess the time-to-peak aortic enhancement in the descending thoracic aorta at the level of the diaphragmatic hiatus. The hepatic arterial phase acquisition was started automatically 12 seconds after the trigger threshold (100 HU) was reached within the aorta. The hepatic venous phase was acquired 40 seconds after the end of the arterial phase. All patients received 150 mL of contrast medium with an iodine concentration of 300 mg/mL (iopamidol 300 mgI/mL; Bracco Diagnostics, Inc, Princeton, NJ), resulting in a total amount of 45 g of iodine. The contrast medium was administered through an 18- to 20-gauge intravenous cannula in the antecubital fossa by means of a dual-chamber mechanical power injector (Empower CTA; Bracco Diagnostics, Inc) at a flow rate of 4 mL/s. Administration of the contrast medium was followed by a 50-mL saline flush using the same injection rate as the contrast media bolus.

Arterial phase imaging was performed in dual-energy mode using the parameters predetermined by the Gemstone Spectral Imaging software (Table 1). As is our normal clinical practice, the technologist selected the most appropriate scan and display field of view for each patient according to the patient's body habitus.

Volume Rendering Reconstructions

A board-certified abdominal imaging fellow processed all dual-energy arterial phase data sets on a dedicated dual-energy workstation (Advantage Windows, AW Server 2, release 5.5; GE Healthcare). Monochromatic image sets at 40, 50, 60, 70, and 80 keV, as well as iodine density images were reconstructed from an iodine-water pair, yielding a total of 174 data sets for all patients (Fig. 1).

Volume-rendered images were subsequently generated from the 40-, 60-, and 80-keV monochromatic images, as well as the iodine density data sets using the volume-rendering tool on the AW thin client. We chose these energy levels because it has been recently shown that 77- and 60-keV data sets approximate mean energy and image appearance of 120- and 80-kVp images, respectively.[5] In an attempt to minimize the effect of recall bias during the qualitative analysis, we decided to avoid additional volume

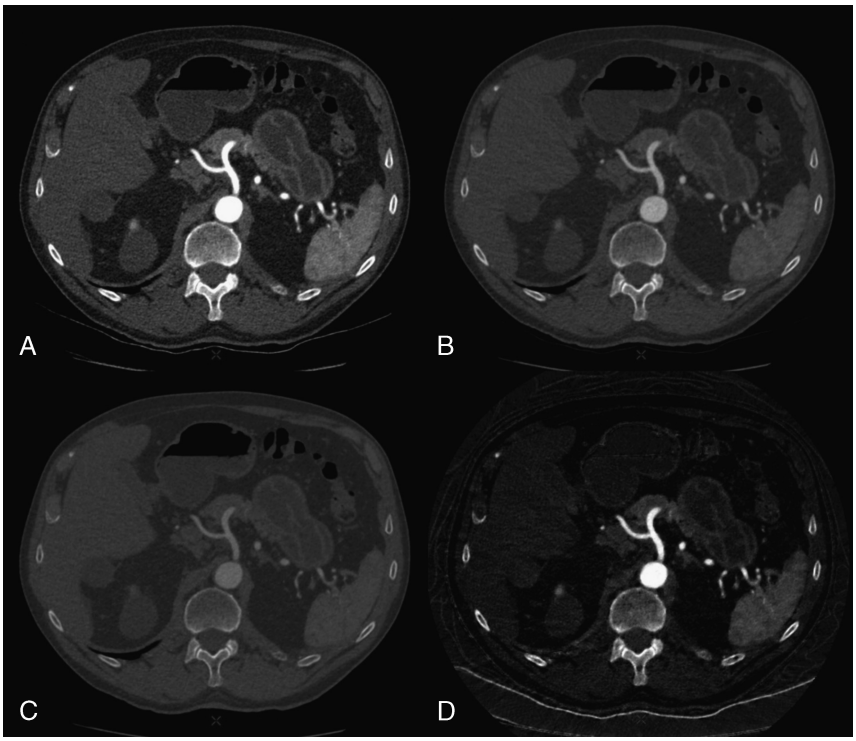

FIGURE 1. Transverse dual-energy MDCT images of the abdomen reconstructed at 40-keV (A), 60-keV (B), and 80-keV (C) synthesized monochromatic energies, as well as using iodine density data sets (D). A–C, For the monochromatic images, the window width and level were held constant at 1450 and 400, respectively. Note the increased arterial attenuation and CNR at 40-keV level compared with 60- and 80-keV levels. Also note the very high CNR on the iodine density image.

rendering reconstructions for the 50- and 70-keV monochromatic data sets.

Because CT numbers change drastically across different monochromatic energy levels, a standardized method of generating opacity attenuation curves for the volume-rendered images was devised. Of note, the upper limit of the opacity curve for all monochromatic image sets was set at the average aortic attenuation (HU) plus 1 SD from a region of interest (ROI) of at least 100 mm^2 drawn in the lumen of the aorta at the level of the celiac artery. For the 40-, 60-, and 80-keV monochromatic images, the lower limit of the opacity curve was set at the average liver attenuation (HU) plus 3 SDs from an ROI measuring at least 400 mm^2 drawn over the liver parenchyma at the level of the celiac artery. For iodine density data sets, the lower limit of the opacity curve was set at the average iodine concentration (mg/mL) of the psoas muscles plus 3 to 5 SDs from an ROI measuring at least 200 mm^2 drawn over the right psoas muscle at the level of the celiac artery. Color for the volume-rendered images was assigned as follows: white at 100% opacity, yellow at 50% opacity, beige at 25% opacity, and red at 0% opacity.

Quantitative Image Analysis

Monochromatic images at 40, 50, 60, 70, and 80 keV, as well as iodine density images, were analyzed on the dual-energy dedicated workstation (Advantage Windows, AW Server 2, release 5.5; GE Healthcare). Manually placed circular ROIs, measuring at least 80 mm^2, were drawn over the aortic lumen and psoas muscle at the level of the right renal artery; mean CT numbers (in HU) were recorded in the aorta and right psoas muscle. The SD of the right psoas muscle was recorded as a surrogate for noise. The same measurements were repeated 2 more times at levels 1 and 2 cm below the origin of the right renal artery. To ensure consistency, all measurements were performed 3 times for each location and average values were calculated. Finally, the anterior-to-posterior and medial-to-lateral diameters of the patient were measured at the level of the L1 vertebral body.

All measurements were performed by an abdominal radiology fellow (blinded to the review process) with 1 year of experience in gastrointestinal and hepatobiliary imaging.

Qualitative Image Analysis

The volume-rendered images (generated from the monochromatic data sets reconstructed at 40, 60, and 80 keV, as well as the iodine density data sets) were scored by 2 independent radiologists (blinded to the review process, respectively) with 8 and 5 years of experience in abdominal and vascular imaging. Image analysis was performed on the same workstation used for the quantitative analysis. Readers were blinded to the reconstruction technique. All patient information was removed from the images. Readers were allowed to make small adjustments from the baseline opacity curve as they saw fit.

The visualization of the hepatic arterial system (ie, proper hepatic, right hepatic, left hepatic, and best visible intrahepatic arteries) and the overall quality of the volume-rendered images were graded using 7- and 5-point Likert scales, respectively (Table 2).[6] Readers were instructed that overall quality scores of 1 or 2 were regarded as nondiagnostic for clinical purposes, whereas scores of 3, 4, or 5 were regarded as diagnostically adequate.

To maximize objectivity and reproducibility of the reader's interpretation of image quality, standardized criteria were presented to the readers in a training session that preceded the first reading. Training consisted of the reader's assessment of 7 representative and criteria-based examples, which were not used in the subsequent analysis. There was no time limit for the readers to complete the training session and the subsequent analysis.

TABLE 2. Likert Scales Adopted for Scoring the Visualization of Hepatic Arterial System and Image Quality

Scale and Score	Description
Visualization of hepatic arteries	
1	Not visible
2	Barely visible and markedly discontinuous (contour difficult to trace)
3	Visible with moderate discontinuity (contour traceable)
4	Visible with mild discontinuity
5	Continuous with moderate wall irregularity
6	Continuous with mild wall irregularity
7	Continuous with smooth walls
Overall image quality	
1	Nondiagnostic image quality, due to inadequate contrast, poor edge definition, or excessive noise and artifacts
2	Suboptimal image quality, due to mild enhancement, impaired edge definition, or moderate noise and artifacts
3	Good image quality, with adequate contrast, edge definition, acceptable noise and artifacts
4	Very good image quality, with good contrast, edge definition better than average, only minimal noise and artifacts
5	Excellent image quality, with excellent contrast, edge definition, lack of evident noise or artifacts

Statistical Analysis

Measurements of aortic attenuation (HU), psoas attenuation (HU), and noise (SD from the psoas muscle ROI) were used to calculate the contrast-to-noise ratio (CNR). Contrast-to-noise ratios were calculated with the formula:

$$\frac{(HU_a - HU_p)}{SD_p}$$

where HU_a is the HU measurement of the aortic ROI, HU_p is the HU measurement of the psoas muscle ROI, and SD_p is the SD from the psoas muscle ROI.

The anterior-to-posterior and medial-to-lateral diameter measurements at the L1 level were used to estimate the body circumference for each patient using the following formula:

$$2\pi\sqrt{\frac{\left(\frac{d_{ap}}{2}\right)^2+\left(\frac{d_{tr}}{2}\right)^2}{2}}$$

where d_{ap} is the anterior-to-posterior diameter of the patient and d_{tr} is the lateral diameter of the patient at the L1 level.

TABLE 3. Aortic Attenuation Values for Different Monochromatic Energy and Iodine-Density Images

Reconstruction Comparison	Statistic	Aortic for First Reconstruction	Aortic for Second Reconstruction	Difference	*P**
0–1	n	29	29	29	
	Mean (SD)	1262 (329)	828 (214)	−434 (115)	
	Min, median, max	621, 1239, 206	414, 807, 1350	−715, −432, −2	<0.001
0–2	n	29	29	29	
	Mean (SD)	1262 (329)	561 (143)	−701 (186)	
	Min, median, max	621, 1239, 206	286, 542, 910	−1E3, −697, −3	<0.001
0–3	n	29	29	29	
	Mean (SD)	1262 (329)	392 (98.7)	−870 (230)	
	Min, median, max	621, 1239, 206	203, 378, 633	−1E3, −861, −4	<0.001
0–4	n	29	29	29	
	Mean (SD)	1262 (329)	283 (70.5)	−979 (259)	
	Min, median, max	621, 1239, 206	146, 272, 455	−2E3, −967, −4	<0.001
0–5	n	29	29	29	
	Mean (SD)	1262 (329)	153 (41.3)	−1E3 (288)	
	Min, median, max	621, 1239, 206	69, 145, 256	−2E3, −1E3, −5	<0.001
1–2	n	29	29	29	
	Mean (SD)	828 (214)	561 (143)	−267 (70.8)	
	Min, median, max	414, 807, 1350	286, 542, 910	−440, −266, −1	<0.001
1–3	n	29	29	29	
	Mean (SD)	828 (214)	392 (98.7)	−436 (115)	
	Min, median, max	414, 807, 1350	203, 378, 633	−717, −430, −2	<0.001
1–4	n	29	29	29	
	Mean (SD)	828 (214)	283 (70.5)	−545 (143)	
	Min, median, max	414, 807, 1350	146, 272, 455	−895, −535, −2	<0.001
1–5	n	29	29	29	
	Mean (SD)	828 (214)	153 (41.3)	−675 (173)	
	Min, median, max	414, 807, 1350	69, 145, 256	−1E3, −654, −3	<0.001
2–3	n	29	29	29	
	Mean (SD)	561 (143)	392 (98.7)	−169 (44.2)	
	Min, median, max	286, 542, 910	203, 378, 633	−277, −164, −8	<0.001
2–4	n	29	29	29	
	Mean (SD)	561 (143)	283 (70.5)	−278 (72.6)	
	Min, median, max	286, 542, 910	146, 272, 455	−455, −269, −1	<0.001
2–5	n	29	29	29	
	Mean (SD)	561 (143)	153 (41.3)	−408 (102)	
	Min, median, max	286, 542, 910	69, 145, 256	−654, −388, −2	<0.001
3–4	n	29	29	29	
	Mean (SD)	392 (98.7)	283 (70.5)	−109 (28.4)	
	Min, median, max	203, 378, 633	146, 272, 455	−178, −105, −5	<0.001
3–5	n	29	29	29	
	Mean (SD)	392 (98.7)	153 (41.3)	−239 (57.8)	
	Min, median, max	203, 378, 633	69, 145, 256	−377, −226, −1	<0.001
4–5	n	29	29	29	
	Mean (SD)	283 (70.5)	153 (41.3)	−130 (29.8)	
	Min, median, max	146, 272, 455	69, 145, 256	−198, −125, −7	<0.001

Reconstructions 0, 1, 2, 3, and 4 corresponded to monochromatic energies of 40, 50, 60, 70, and 80 keV. Reconstruction 5 corresponded to iodine-density images.

**P* value based on Wilcoxon signed rank test of median difference equal to zero.

TABLE 4. Noise Values for Different Monochromatic Energy and Iodine-Density Images

Reconstruction Comparison	Statistic	Noise for First Reconstruction	Noise for Second Reconstruction	Difference	*P**
0–1	n	29	29	29	
	Mean (SD)	65 (20.2)	45.8 (16.1)	−19 (4.9)	
	Min, median, max	32, 63, 102	21, 42, 75	−31, −19, −11	<0.001
0–2	n	29	29	29	
	Mean (SD)	65 (20.2)	38.6 (15)	−27 (7.2)	
	Min, median, max	32, 63, 102	17, 34, 67	−46, −26, −15	<0.001
0–3	n	29	29	29	
	Mean (SD)	65 (20.2)	25.7 (8.8)	−39 (11.5)	
	Min, median, max	32, 63, 102	13, 24, 41	−61, −39, −19	<0.001
0–4	n	29	29	29	
	Mean (SD)	65 (20.2)	24.1 (6.8)	−41 (13.7)	
	Min, median, max	32, 63, 102	13, 24, 37	−67, −38, −19	<0.001
0–5	n	29	29	29	
	Mean (SD)	65 (20.2)	6.9 (2.3)	−58 (18.1)	
	Min, median, max	32, 63, 102	4, 6, 12	−93, −57, −28	<0.001
1–2	n	29	29	29	
	Mean (SD)	45.8 (16.1)	38.6 (15)	−7.3 (2.6)	
	Min, median, max	21, 42, 75	17, 34, 67	−14, −8, −2	<0.001
1–3	n	29	29	29	
	Mean (SD)	45.8 (16.1)	25.7 (8.8)	−20 (7.3)	
	Min, median, max	21, 42, 75	13, 24, 41	−35, −18, −9	<0.001
1–4	n	29	29	29	
	Mean (SD)	45.8 (16.1)	24.1 (6.8)	−22 (9.9)	
	Min, median, max	21, 42, 75	13, 24, 37	−42, −20, −8	<0.001
1–5	n	29	29	29	
	Mean (SD)	45.8 (16.1)	6.9 (2.3)	−39 (13.9)	
	Min, median, max	21, 42, 75	4, 6, 12	−63, −37, −18	<0.001
2–3	n	29	29	29	
	Mean (SD)	38.6 (15)	25.7 (8.8)	−13 (6.6)	
	Min, median, max	17, 34, 67	13, 24, 41	−28, −10, −5	<0.001
2–4	n	29	29	29	
	Mean (SD)	38.6 (15)	24.1 (6.8)	−15 (9.4)	
	Min, median, max	17, 34, 67	13, 24, 37	−38, −12, −4	<0.001
2–5	n	29	29	29	
	Mean (SD)	38.6 (15)	6.9 (2.3)	−32 (12.8)	
	Min, median, max	17, 34, 67	4, 6, 12	−57, −28, −14	<0.001
3–4	n	29	29	29	
	Mean (SD)	25.7 (8.8)	24.1 (6.8)	−1.6 (2.9)	
	Min, median, max	13, 24, 41	13, 24, 37	−10, −1, 2	0.018
3–5	n	29	29	29	
	Mean (SD)	25.7 (8.8)	6.9 (2.3)	−19 (6.7)	
	Min, median, max	13, 24, 41	4, 6, 12	−32, −18, −8	<0.001
4–5	n	29	29	29	
	Mean (SD)	24.1 (6.8)	6.9 (2.3)	−17 (4.9)	
	Min, median, max	13, 24, 37	4, 6, 12	−28, −17, −9	<0.001

Reconstructions 0, 1, 2, 3, and 4 corresponded to monochromatic energies of 40, 50, 60, 70, and 80 keV. Reconstruction 5 corresponded to iodine-density images.

**P* value based on Wilcoxon signed rank test of median difference equal to zero.

For each keV level, the 3 quantitative measurements of aortic attenuation, noise, and CNR were averaged and used in the analyses. The significance of pairwise differences for these measurements between keV levels was assessed using the Wilcoxon signed rank test of median difference equal to zero. The subjective reader scores for visibility of the common hepatic, right hepatic, left hepatic, and intrahepatic arteries, as well as overall image quality were averaged separately for each keV level and used in the analyses. The significance of pairwise differences between keV levels for these measurements was assessed using the Wilcoxon signed rank test of median difference equal to zero.

In addition, a bivariate fit analysis was performed by plotting the body circumference against the slope of the line for CNR vs keV for each patient.

RESULTS

Quantitative Analysis

When 40-keV data sets were compared with 80-keV data sets, both aortic attenuation and noise increased progressively with decreasing monochromatic keV settings, with a net increase of 346% and 170%, respectively (Tables 3 and 4; $P < 0.001$ for both comparisons; Fig. 2). Noise was significantly lower for the iodine density compared with all monochromatic data sets (Table 4; $P < 0.001$ for all comparisons). The estimated average iodine content of the abdominal aorta was 153 ± 42 mg/mL on the iodine density data sets.

Aortic CNR increased progressively with decreasing monochromatic keV settings (Table 5), with a net increase of 89% when 40-keV data sets were compared with 80-keV data sets ($P < 0.001$; Fig. 2). There was no significant difference in aortic CNR between 40- and 60-keV data sets. The magnitude of increase in aortic CNR at lower monochromatic energies was greater for smaller compared with patients with larger body size, as indicated by the steeper slope of the regression lines in smaller patients (Fig. 3). The slope of the regression lines was nearly flat in patients with body circumference of 100 cm or larger, indicating minimal changes in aortic CNR among different monochromatic energies. Aortic CNR was significantly higher for the iodine density compared with all monochromatic data sets (Table 5; $P < 0.001$ for all comparisons).

Qualitative Analysis

The readers' scores for image quality showed improved visibility of the common hepatic, as well as the right and left intrahepatic arteries on volume-rendered images generated at lower monochromatic keV settings (Table 6). This improvement was statistically significant when 40-keV data sets were compared with 80-keV data sets ($P < 0.001$). There was no significant difference in readers' scores between 40- and 60-keV data sets. For all hepatic arterial segments, the visualization of the hepatic arterial anatomy was rated significantly worse for the iodine density compared with all monochromatic data sets (Table 6; $P < 0.001$ for all comparisons).

Readers' perception of overall image quality improved progressively at lower monochromatic keV settings. This improvement was significant when 40-keV data sets were compared with 80-keV data sets ($P < 0.001$). Overall perception of image quality was significantly worse for the iodine density compared with all monochromatic data sets (Table 6; $P < 0.001$ for all comparisons). More importantly, overall image quality was diagnostic for all monochromatic data sets, but nondiagnostic for iodine density data sets (Fig. 4).

DISCUSSION

Our study suggests that lower-energy synthesized monochromatic images maximize the magnitude of arterial enhancement and have improved reader's perception of image quality during the interpretation of hepatic arterial MDCT angiography examinations. Our data showed significantly higher arterial attenuation and CNR for synthesized monochromatic data sets in the 40- to 60-keV range. This improvement, which is likely explained by higher x-ray absorption by iodine at x-ray energies closer to the iodine *k* edge (33.2 keV), was accompanied by a significant improvement in the reader's perception of image quality for volumetric renderings of the hepatic arterial anatomy. Our data corroborates the results of previous studies, which showed a significant improvement in arterial CNR and image quality of volumetric renderings at synthesized monochromatic images between 40 and 50 keV.[7–9]

Although our results seem to suggest that synthesized monochromatic energies between 40 and 60 keV should be used clinically during interpretation of hepatic MDCT angiography examinations, this observation should be interpreted with caution. Our data showed that despite a significant improvement in arterial CNR, lower-energy synthesized monochromatic images yielded a significant increase in noise. Although our data indicate that the detrimental effect of noise on the quality of volumetric renderings may not be

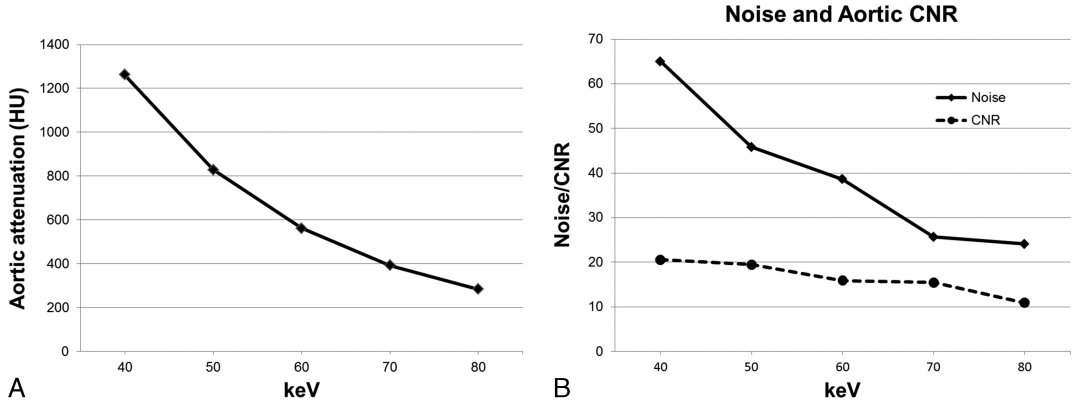

FIGURE 2. (A) Aortic attenuation and (B) noise and aortic CNR for different monochromatic energy levels.

TABLE 5. Contrast-to-Noise Values for Different Monochromatic Energy and Iodine-Density Images

Reconstruction Comparison	Statistic	CNR for First Reconstruction	CNR for Second Reconstruction	Difference	*P**
0–1	n	29	29	29	
	Mean (SD)	20.6 (12.6)	19.5 (12.5)	−1 (0.8)	
	Min, median, max	6, 17, 60	5, 16, 58	−3, −1, 1	<0.001
0–2	n	29	29	29	
	Mean (SD)	20.6 (12.6)	15.9 (10.4)	−4.7 (2.6)	
	Min, median, max	6, 17, 60	4, 13, 48	−12, −4, −2	<0.001
0–3	n	29	29	29	
	Mean (SD)	20.6 (12.6)	15.5 (9.7)	−5.1 (3)	
	Min, median, max	6, 17, 60	4, 12, 45	−15, −4, −2	<0.001
0–4	n	29	29	29	
	Mean (SD)	20.6 (12.6)	10.9 (6.2)	−9.7 (6.4)	
	Min, median, max	6, 17, 60	3, 9, 29	−31, −8, −3	<0.001
0–5	n	29	29	29	
	Mean (SD)	20.6 (12.6)	24.7 (14.2)	4.2 (4.3)	
	Min, median, max	6, 17, 60	6, 23, 65	−3, 4, 16	<0.001
1–2	n	29	29	29	
	Mean (SD)	19.5 (12.5)	15.9 (10.4)	−3.7 (2.3)	
	Min, median, max	5, 16, 58	4, 13, 48	−10, −3, −1	<0.001
1–3	n	29	29	29	
	Mean (SD)	19.5 (12.5)	15.5 (9.7)	−4 (2.8)	
	Min, median, max	5, 16, 58	4, 12, 45	−13, −3, −1	<0.001
1–4	n	29	29	29	
	Mean (SD)	19.5 (12.5)	10.9 (6.2)	−8.6 (6.4)	
	Min, median, max	5, 16, 58	3, 9, 29	−29, −6, −2	<0.001
1–5	n	29	29	29	
	Mean (SD)	19.5 (12.5)	24.7 (14.2)	5.2 (4.3)	
	Min, median, max	5, 16, 58	6, 23, 65	−1, 5, 18	<0.001
2–3	n	29	29	29	
	Mean (SD)	15.9 (10.4)	15.5 (9.7)	−0.4 (1.2)	
	Min, median, max	4, 13, 48	4, 12, 45	−3, 0, 2	0.245
2–4	n	29	29	29	
	Mean (SD)	15.9 (10.4)	10.9 (6.2)	−5 (4.4)	
	Min, median, max	4, 13, 48	3, 9, 29	−19, −4, 0	<0.001
2–5	n	29	29	29	
	Mean (SD)	15.9 (10.4)	24.7 (14.2)	8.9 (5.1)	
	Min, median, max	4, 13, 48	6, 23, 65	2, 8, 25	<0.001
3–4	n	29	29	29	
	Mean (SD)	15.5 (9.7)	10.9 (6.2)	−4.6 (3.6)	
	Min, median, max	4, 12, 45	3, 9, 29	−16, −3, 0	<0.001
3–5	n	29	29	29	
	Mean (SD)	15.5 (9.7)	24.7 (14.2)	9.2 (5.8)	
	Min, median, max	4, 12, 45	6, 23, 65	1, 8, 27	<0.001
4–5	n	29	29	29	
	Mean (SD)	10.9 (6.2)	24.7 (14.2)	13.8 (8.6)	
	Min, median, max	3, 9, 29	6, 23, 65	2, 13, 37	<0.001

Reconstructions 0, 1, 2, 3, and 4 corresponded to monochromatic energies of 40, 50, 60, 70, and 80 keV. Reconstruction 5 corresponded to iodine-density images.

**P* value based on Wilcoxon signed rank test of median difference equal to zero.

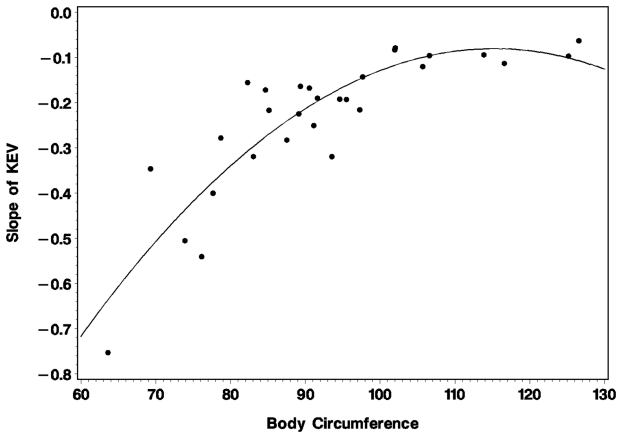

FIGURE 3. Bivariate fit analysis for the slopes of the aortic CNR as a function of monochromatic energy level (*y* axis) and body circumference (*x* axis) for each patient.

significant, a finding that is not surprising considering the smaller contribution of noise during the interpretation of high-contrast diagnostic tasks, [5] we did not investigate the impact of noise on the radiologist's interpretation of coexistent nonvascular findings. This is an important limitation of our study as previous evidence has suggested that higher-energy synthesized monochromatic images (in the range of 60 and 70 keV) may be better for routine abdominal applications.[1–4] This energy range corresponds to the midpoint between the mean energies of the 2 x-ray spectra (80 and 140 kVp), yielding the lowest noise in the synthesized monochromatic data sets.[1–4]

Another noteworthy finding in our study was the impact of body size on the selection of the optimal monochromatic energy level, a relationship that has not been investigated before. The results of our linear regression analysis showed that the improvement in arterial CNR at lower monochromatic energies was almost negligible in larger-sized patients. These data are in agreement with the findings of a recent phantom experiment by Yu and colleagues, [3] suggesting the need for higher monochromatic energy levels to optimize iodine CNR with increasing phantom size. This effect is likely secondary to an incomplete correction of beam hardening in dual-energy data sets from larger patients. Collectively, these findings support the theory of multiple factors by Yu et al[3] influencing the selection of an optimal monochromatic energy level, including phantom size, partitioning of the radiation dose between low- and high-energy scans, and the image quality metrics to be optimized.

Besides the retrospective nature, some potential limitations of our study merit consideration. First, this investigation reflects our preliminary experience in a small number of patients. Second, we did not assess the impact of both improved vascular CNR and better visualization of the hepatic arterial anatomy on readers' diagnostic performance for detection of vascular pathology. Third, we intentionally excluded the 140-kVp polychromatic data set of the dual-energy acquisition from our data analysis primarily because of the inherently poor low-contrast detectability. This decision was also motivated by the notion that tube voltages lower than 140 kVp should be selected for MDCT angiography applications.[10–12] Future studies are warranted to compare optimal synthesized monochromatic images with single-energy MDCT acquisitions at lower tube voltages.

In summary, our study results suggest that synthesized monochromatic images between 40 and 60 keV maximize the magnitude of arterial enhancement and improve visualization of hepatic arterial anatomy at dual-energy MDCT angiography of the liver. Our data also suggest that increasing body sizes

TABLE 6. Qualitative Assessment of Image Quality of Volume-Rendered Images of the Hepatic Arteries for Different Monochromatic Energy and Iodine-Density Images

Reconstruction	Statistic	Reconstruction 1	Reconstruction 2	Difference	*P**
40–60 keV	n	29	29	29	
	Mean (SD)	6.2 (0.7)	6.1 (0.8)	−0.1 (0.5)	
	Min, median, max	5, 7, 7	4, 6, 7	−1, 0, 1	0.361
40–80 keV	n	29	29	29	
	Mean (SD)	6.2 (0.7)	5.7 (0.8)	−0.4 (0.5)	
	Min, median, max	5, 7, 7	4, 6, 7	−2, −1, 1	<0.001
40 keV–iodine	n	29	29	29	
	Mean (SD)	6.2 (0.7)	5.4 (1)	−0.8 (0.7)	
	Min, median, max	5, 7, 7	3, 6, 7	−3, −1, 1	<0.001
60–80 keV	n	29	29	29	
	Mean (SD)	6.1 (0.8)	5.7 (0.8)	−0.4 (0.5)	
	Min, median, max	4, 6, 7	4, 6, 7	−2, −1, 1	<0.001
60 keV–iodine	n	29	29	29	
	Mean (SD)	6.1 (0.8)	5.4 (1)	−0.7 (0.6)	
	Min, median, max	4, 6, 7	3, 6, 7	−2, −1, 0	<0.001
80 keV–iodine	n	29	29	29	
	Mean (SD)	5.7 (0.8)	5.4 (1)	−0.4 (0.6)	
	Min, median, max	4, 6, 7	3, 6, 7	−2, −1, 1	0.008

*Wilcoxon signed rank test of median difference equal to zero.

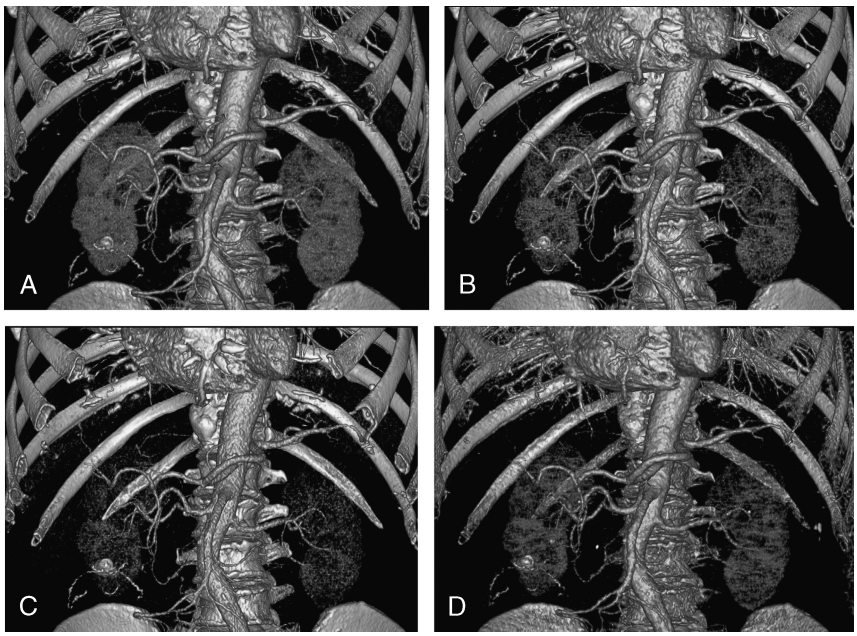

FIGURE 4. Coronal volume-rendered images of the abdominal aorta and aortic branches obtained using optimized opacity curves from the 40-keV (A), 60-keV (B), and 80-keV (C) synthesized monochromatic data sets, as well as the iodine density data set (D). Note the improved visibility and smoother appearance of the vascular contour at 40 keV for both large and small arteries.

may counteract the benefits of using lower synthesized monochromatic energies.

REFERENCES

1. Yu L, Leng S, McCollough CH. Dual-energy CT-based monochromatic imaging. *AJR Am J Roentgenol*. 2012;199:S9–S15.
2. Matsumoto K, Jinzaki M, Tanami Y, et al. Virtual monochromatic spectral imaging with fast kilovoltage switching: improved image quality as compared with that obtained with conventional 120-kVp CT. *Radiology*. 2011;259:257–262.
3. Yu L, Christner JA, Leng S, et al. Virtual monochromatic imaging in dual-source dual-energy CT: radiation dose and image quality. *Med Phys*. 2011;38:6371–6379.
4. Venema HW. Virtual monochromatic spectral imaging with fast kilovoltage switching should not be used as standard CT imaging modality. *Radiology*. 2011;260:916–917.
5. Kulkarni NM, Sahani DV, Desai GS, et al. Indirect computed tomography venography of the lower extremities using single-source dual-energy computed tomography: advantage of low-kiloelectron volt monochromatic images. *J Vasc Interv Radiol*. 2012;23:879–886.
6. Mitsumori LM, Shuman WP, Busey JM, et al. Adaptive statistical iterative reconstruction versus filtered back projection in the same patient: 64 channel liver CT image quality and patient radiation dose. *Eur Radiol*. 2012;22:138–143.
7. Yuan R, Shuman WP, Earls JP, et al. Reduced iodine load at CT pulmonary angiography with dual-energy monochromatic imaging: comparison with standard CT pulmonary angiography—a prospective randomized trial. *Radiology*. 2012;262:290–297.
8. Hu D, Yu T, Duan X, et al. Determination of the optimal energy level in spectral CT imaging for displaying abdominal vessels in pediatric patients. *Eur J Radiol*. 2014;83:589–594.
9. He J, Ma X, Wang Q, et al. Spectral CT demonstration of the superior mesenteric artery: comparison of monochromatic and polychromatic imaging. *Acad Radiol*. 2014;21:364–368.
10. Wintermark M, Maeder P, Verdun FR, et al. Using 80 kVp versus 120 kVp in perfusion CT measurement of regional cerebral blood flow. *AJNR Am J Neuroradiol*. 2000;21:1881–1884.
11. Bahner ML, Bengel A, Brix G, et al. Improved vascular opacification in cerebral computed tomography angiography with 80 kVp. *Invest Radiol*. 2005;40:229–234.
12. Waaijer A, Prokop M, Velthuis BK, et al. Circle of Willis at CT angiography: dose reduction and image quality—reducing tube voltage and increasing tube current settings. *Radiology*. 2007;242:832–839.